



# Performance comparison between standard and magnetically shielded 200 W Hall thrusters with BN-SiO<sub>2</sub> and graphite channel walls



Lou Grimaud\*, Stéphane Mazouffre

CNRS, ICARE, UPR3021, 1C Av. Recherche Scientifique, Orléans Cedex 2, France

## ARTICLE INFO

### Keywords:

Hall thruster  
Electric propulsion  
Magnetic shielding  
Wall materials

## ABSTRACT

Magnetic shielding is a specific magnetic topology that can increase the lifespan of Hall thrusters by an order of magnitude. Magnetically shielded thrusters have similar performances as standard unshielded thrusters in the 5–15 kW power range. A comparison of the performances of two 200 W shielded (ISCT200-MS) and unshielded (ISCT200-US) Hall thrusters is presented here. The effects of replacing the usual BN-SiO<sub>2</sub> walls with graphite are investigated on both thrusters. The ISCT200-US thruster has a peak anode efficiency of 39% and a specific impulse of 1400 s at 250 W with the ceramic discharge channel. However with graphite wall, the discharge current increases by 25% which reduces the efficiency down to 31% (1360 s specific impulse). The ISCT200-MS performances are significantly lower than the ISCT200-US at similar operating points. It only reaches 24% anode efficiency and 1020 s specific impulse at 250 W. The switch to graphite has little effects on its performances below 300 V. The lower performances are due to a low propellant utilization. We propose that this low propellant utilization is caused by lower ionization near the walls which has a large impact in small thrusters due to their higher surface to volume ratio.

## 1. Introduction

Hall thrusters are one of the most widely used electric propulsion system for space applications [1]. They benefit from their high thrust to power ratio and a moderate specific impulse that makes them particularly well suited for missions within earth's sphere of gravitational influence.

One of limiting factor of Hall thruster (HT) usage is their limited lifespan caused by the wall erosion. This erosion is particularly severe in small thrusters ( $\leq 500$  W) where the surface to volume ratio of the discharge channel is high. Such thrusters rarely last more than 3000 h [2] while kilowatt class HT often achieve 10,000 h long lifespan [3].

Increasing the lifespan of HT would enable a number of missions for this technology. On the high power side ( $\geq 5$  kW) the lifespan can be limiting for all electric satellite platform as the electric orbit raising considerably increase the total firing time. It would also make HT competitive for exploration missions such as the now canceled robotic segment of the Asteroid Redirect Mission [4]. For low power units a longer lifespan would allow the use of HT for very low Earth orbit drag compensation applications. It would also remove a failure mechanism that could prevent end of life disposal of the satellite.

One solution, initially investigated by the Jet Propulsion Laboratory, is to use a “magnetic shielding” (MS) topology [5]. This

technique prevents the flow of the high energy ions responsible for erosion toward the walls. This has been shown to effectively reduce erosion by two orders of magnitude. More details on how magnetically shielded thrusters operate will be provided in section 2.

Results presented here are a direct comparison between a magnetically shielded (MS) and an unshielded (US) version of the same thruster with a nominal operating power of 200 W. Both thrusters are tested with a BN-SiO<sub>2</sub> (M26 grade from Saint Gobain) and a graphite discharge channel. First will be presented the concept of magnetic shielding as well as a short review of the principle of magnetic shielding applied to Hall thrusters and influence of the discharge channel material on their operation. The experimental setup used in this test campaign will be discussed in section 3. Lastly the results will be presented and discussed in section 4.

## 2. Background

### 2.1. Magnetic shielding operating principle

A classical Hall thruster is a  $E \times B$  plasma device. An almost radial magnetic field is induced in an annular discharge chamber. At the back of the chamber a neutral gas (Xenon in most cases) is injected and an anode is placed. An external cathode is used to produce electrons. Some

\* Corresponding author.

E-mail address: [lou.grimaud@cnrs-orleans.fr](mailto:lou.grimaud@cnrs-orleans.fr) (L. Grimaud).

of these electrons travel toward the anode and are trapped by the magnetic barrier in an azimuthal Hall current. This Hall current ionize the atoms injected by the anode. The low electron diffusion rate in that barrier makes it an area of high (axial) ohmic resistance and thus localizes the potential drop applied between the cathode and the anode. This electric field accelerates the ions. The intensity of the magnetic field is chosen such that only the electrons are magnetized.

Due to the high mobility of the electrons along the magnetic field lines, and the relative radial uniformity of the plasma density, those can be considered equipotential and isotherm as a first order approximation. This has been used for years to shape the electric field in a Hall thruster and focus the ion beam. It is often referred to as a “plasma lens” effect [6–10].

In 2010, surprising results were obtained during lifetime testing of the BPT-4000 Hall thruster [11]: after 5600 h of firing erosion stopped. After investigation the relationship between the magnetic topology and the physical shape of the discharge channel was found to be responsible for this erosion-less state. The research teams at the Jet Propulsion Laboratory and Aerojet named that configuration “magnetic shielding” (MS). The difference between a classical unshielded (US) and shielded configuration is illustrated in Fig. 1. The concept takes advantage of the properties of the magnetic field lines to reduce both the ion energy and ion flux impacting the walls. A field line tangent to the wall is created between the top of the thruster and the anode area at the back of the channel. This lined, called the “grazing line” ensure that the area along the wall has a layer of cold electrons ( $\sim 5$  eV) originating from the anode region. That lower electron temperature reduces the sheath potential drop at the wall and thus the energy of the ions accelerated through that sheath.

In order to produce that grazing line the maximum of the magnetic field along the center of the discharge channel needs to be pushed downstream. This results in a downstream shift of the ionization and acceleration regions, further reducing the density and average energy of the ions.

## 2.2. Previous work on low power magnetically shielded thruster

Experiments on the H6MS thruster have shown similar performance as the unshielded (US) H6 thruster [12]. The 12.5 kW HERMeS MS-HT also presents very good performances [13].

Low power Hall thruster in the 100–400 W range are usually limited to lower efficiencies. An anode efficiency map of number of low power Hall thrusters can be found in the appendix 5.1. Most of the thrusters found in the literature hover around 35–40% efficiency in the in the 200–300 W range. The BHT-200 and the CAMILA-HT-55 are two notable exceptions with efficiencies approaching 50%.

One of the reasons often put forward to explain the lower efficiency of small thrusters is their higher surface to volume ratio which promotes energy losses to the walls. One of the solution proposed to solve this issue is to increase the relative width of the discharge channel [14–16]. Since the magnetic shielding topology reduces the interactions between the plasma and the walls it has the potential to also reduce

losses in those small thrusters.

This however has not been the case for the first versions of the low power MaSMi-40 and MaSMi-60 magnetically shielded HTs [17]. Their efficiency is markedly lower than equivalent unshielded thrusters (see Fig. 9). Conversano explains that low efficiency by a combination of low propellant utilization due to inefficient gas injection, weak magnetic field and high field gradients as well as high divergence caused by the magnetic shielding topology [18,19]. Subsequent developments with the MaSMi-60-LM2 [20] and MaSMi-DM [21] have raised the performance of this thruster to 45% anode efficiency at 500 W.

The goal of this study is to compare the performance of a traditional unshielded thruster with a shielded version as well as with other similarly sized Hall thrusters. It should be noted that both those thrusters are laboratory prototypes that have not been optimized for performance.

The results presented here are part of a more general study on low power magnetically shielded thrusters. A 200 W permanent magnets, magnetically shielded Hall thruster named the ISCT200-MS was built with the same dimensions and magnetic field strength as the ISCT200-US. The shape of the radial magnetic field intensity along the center of the discharge channel was also conserved. However the position of this profile had to be changed to accommodate the magnetic shielding topology. The similarity was kept in order to compare the capability of the two thrusters. The original ISCT200-US (previously called PPI-Mag) was a thruster used to investigate the effect of the width of the high magnetic field area [10].

An initial mapping effort of the discharge envelope was first presented in 2016 [22,23]. The results demonstrated that the discharge currents were reasonably similar in both thrusters for a given discharge voltage and mass flow.

A series of plume measurements conducted in the NExET vacuum chamber showed that the ISCT200-US and ISCT200-MS both have similar divergence angle but that the shielded thruster does not ionize the propellant as well as its unshielded counterpart [22,24].

The mechanisms of magnetic shielding in a small thruster were also investigated [25]. Laser induced fluorescence spectroscopy revealed that in the MS-HT the acceleration region is situated primarily outside the thruster. The ionization region is also shifted downstream which overall reduces the density of energetic ions responsible for the erosion of the discharge channel.

The ion velocity distribution function near the walls shows that the ions are not accelerated toward the walls either. This is presumably due to the magnetic field lines parallel to the wall both reducing the electron temperature (and thus the sheath potential) and directing the electric field away from them. The laser induced fluorescence also revealed some ions coming toward the inner magnetic pole. While the velocity of the ions is not extremely high (in the order of 5 km/s) it could be responsible for the tenuous erosion observed there. The origin and the mechanism responsible for accelerating those ions could not be determined by those measurements.

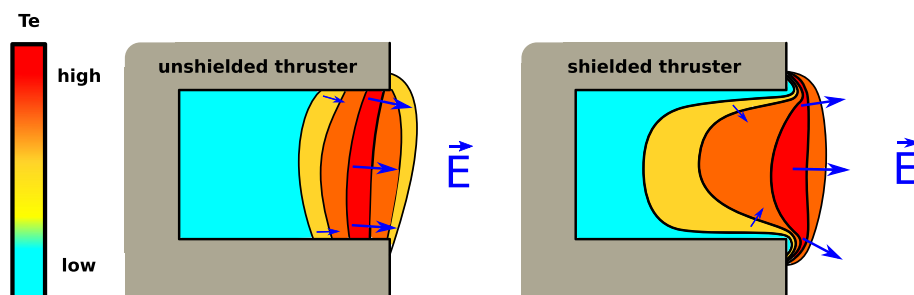


Fig. 1. Comparison between classical and magnetic shielding configurations, the black lines represent the magnetic field lines.

### 2.3. Alternative wall materials and magnetic shielding

#### 2.3.1. Motivations for alternative materials

More recently we have studied the influence of the wall material on the discharge characteristics of both thrusters [24]. Since the magnetic shielding topology limits the electric field intensity near the walls and reduces the ion density in this region [25] it stands to reason that the thruster should be less sensitive to the wall material.

Goebel et al. [26] first attempted to replace the usual boron nitride compound with graphite on the 6 kW magnetically shielded H6MS Hall thruster. Their results show that the discharge current is mostly undisturbed by the change of material and that the anode efficiency is only a couple of percents lower with this material than with the classical boron nitride walls.

This result is remarkable. Graphite seriously deteriorates performances in an unshielded thruster. Gascon et al. [27,28] showed this when they studied the performances of the 1.5 kW SPT-100-ML with different wall materials. This study included the use of borosil (BN-SiO<sub>2</sub>), alumina, silicon carbide and graphite discharge channel walls. While the thrust versus discharge voltage behavior was not perturbed much by the change in material, they observed up to 25% increase of the mean discharge current as well as an increase in its oscillations. This had for effect to reduce the anode efficiency from 50% in borosil to 30% with graphite.

Other efforts in using conducting materials in HT discharge channels include a 200 W thruster from the Harbin Institute of Technology [29]. This thruster has a magnetic topology designed to push the discharge outside the thruster and is presented as a “no wall loss” thruster [30]. Tests with a titanium discharge channel have demonstrated an anode efficiency of 34%. Earlier tests were also conducted at Princeton with various configurations of short graphite rings [31].

The similarities between our two thrusters allow us to directly compare the influence of the wall material on equivalent US and MS Hall thrusters.

From an engineering point of view graphite is an interesting material for two reasons. Firstly, it has a lower sputter yield than boron nitride compounds [32] by a factor of 2–3 at the relevant energies. This means that any residual erosion in magnetic shielding configuration could be mitigated even more by replacing the wall material. The second reason is practical one for thruster ground testing. Back sputtered material from the chamber, usually composed of carbon compounds, tends to deposit on the surfaces of the thruster and change the properties of the walls. In a magnetically shielded thruster this layer is not cleaned by erosion. Since this phenomenon is not present in space, it violates the “test as you fly” philosophy when MS-HT are ground tested. Showing that carbon walls have no influence on the thruster would answer these concerns.

#### 2.3.2. Previous results

Our first series of measurements shows no significant difference when the ISCT200-MS is fired with graphite and boron nitride (Saint-Gobain’s BN M26 grade) walls [24]. Both the mean discharge current and its dynamics are similar. The plume is not affected either. Lastly the electric field stays at the same position (ie near the maximum of the magnetic field).

This is a stark contrast with the US-HT. The switch to graphite produces a 20–30% higher discharge current at similar voltage and mass flow. The dynamics are also significantly altered with more pronounced oscillations with the conducting graphite. The accelerating electric field is also stretched out and push downstream. Lastly a larger divergence angle and ion current were measured in the graphite configuration.

The results presented here have for objective to conclude this study by measuring the thrust of the US and MS Hall thrusters with graphite and BN-SiO<sub>2</sub> walls. This will highlight any effect of the wall materials on the specific impulse and anode efficiency of classical and shielded

low power thrusters.

## 3. Experimental setup

### 3.1. PIVOINE 2G test facility

The PIVOINE 2G test facility is setup around a 4 m × 2.2 m cylindrical vacuum chamber. It is outfitted with a 220000 l/s cryogenic pumping system sized for Hall thrusters ranging from 1 to 20 kW. This allowed us to maintain a very good vacuum during the whole test campaign. All the measurements presented in this work were performed at a xenon pressure between 5 and 7.5 × 10<sup>-6</sup> mbar. This is below the threshold at which pressure effects become significant [33]. The large chamber relative to the thruster size and power also ensures minimal boundary effects from the grounded chamber. During operation the thruster is positioned on the axis of the vacuum chamber, 0.5 m from the airlock entrance.

The thrusters were fired with an oversized 5 A class cathode [34,35]. The cathode is placed below the thruster with its orifice 15 cm from the thruster centerline and 5 cm downstream of the exit plane. It is angled 45° with respect to the thruster axis. All the figures presented in this article do not take into account the cathode heating power or the cathode mass flow.

Both thruster and cathode are fired with 99.998% pure xenon.

### 3.2. Plume measurements

Plumes measurements were performed with 15 mm diameter Faraday cup probe. This probe is mounted on a rotating arm 70 cm from the thruster exit plane (approximately 20 thruster diameters). The probe surface is polarized by a Keithley 2410 source meter that also measured the collected ion current. More details on the probe design and utilization can be found in Ref. [33].

The arm is rotating on a 180° arc in front of the thruster and the ion current is measured over 70 individual points with 2° steps between -50 and 50°. An example of the profile measured can be seen on Fig. 2.

The data collected is not corrected for charge exchange or any other effects. The total ion current is computed by integrating the ion current over the hemisphere facing the thruster. The divergence angle is defined as the half angle of the cone containing 90% of the collected ion current. We define the beam efficiency  $\eta_l$  as the ratio of collected ion current over the total discharge current. The propellant utilization  $\eta_{prop}$  is the ratio of collected ions (assuming those are singly charged) over the number of neutral atoms injected at the anode. It is computed using equation (1) with  $I_b$  being the beam current,  $M_{Xe}$  the mass on an atom of xenon and  $N_a$  Avogadro’s constant. The mean charge of the ion  $q_{mean}$  is assumed to be 1  $e$  for the results presented in section 4.2. This is a strong assumption, especially on a magnetically shielded thruster and it will be discussed with the results in section 4.3.1. However since no data on the mean charge of the ions is available on the thrusters and the materials studied, we cannot confidently estimate what the real mean

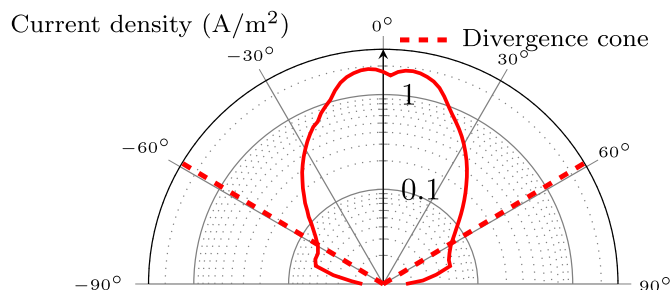


Fig. 2. Ion current profile for the US-HT in BN-SiO<sub>2</sub> at 200 V and 1.2 mg/s collected 70 cm from the thruster. The dashed line represent the divergence angle  $\alpha_d$ .

ion charge is.

$$\eta_{prop} = \frac{I_b \cdot M_{Xe} \cdot N_a}{q_{mean} \cdot \dot{m}_a} \quad (1)$$

Measurements were performed for each thruster at 200 V, 1 and 1.2 mg/s anode mass flow.

### 3.3. Thrust stand

The thrust stand in PIVOINE 2G is a simple pendulum design. The thruster is mounted on a titanium structure suspended by three braided steel wires and connected with a flexible PCB. The displacement of the thrust stand is measured by a capacitive sensor with a resolution of 0.2  $\mu\text{m}$ .

The thrust stand is fitted with a system of reference masses for calibration. A first 1 h “burn in” test fire is done in order to fully outgas the discharge channels. For each operating conditions the thruster is fired for at least 10 min. After this waiting period we allow the thruster to stabilize by looking at both the variation of the mean discharge current and the current oscillations on an oscilloscope. The discharge is considered stable if the dynamics and the mean value do not change over a 2 min period. While this is not strictly sufficient for a true thermal equilibrium to be reached it ensures a stable discharge mode. The position of the thrust stand is then recorded for several minutes. The thruster is shut down and the two reference masses are hung. For each configurations (no mass, mass 1, mass 1 and mass 2) the position of the thrust stand is measured. These three values are used as calibration points. The thrust stand is not temperature controlled. Thrust stand calibrations are done after each measurements point in order to minimize thermal drift effects. Over an individual measurement period the thermal drift appears to be linear with respect to time. This linear trend is subtracted from the results. While this processing technique further increase the width of the error bars it greatly reduce systematic error.

The thrust stand, like the rest of the PIVOINE 2G facility was designed for thruster between 1 and 20 kW (ie thrust ranging from 50 to 1000 mN). As such the precision on the measured thrust is only typically around  $\pm 0.5$  mN for thrust values between 5 and 15 mN. Uncertainty bounds are computed individually for each measurements by taking into account uncertainty in the position of the thrust stand, the calibration masses, the discharge current and voltage as well as in the mass flow. Most of the uncertainty is due to the position sensor resolution.

Thrust measurement were performed for anode mass flows of 0.8, 1 and 1.2 mg/s and discharge voltages of 150, 200, 250 and 300 V.

## 4. Results and discussion

### 4.1. Thrust and efficiency

#### 4.1.1. Unshielded thruster

The thrust versus voltage, and specific impulse versus voltage curves for the different anode mass flows and channel materials are shown in Fig. 3 b) and 3 c). The thrust ranges between 6 and 16 mN and the ISP between 600 and 1400 s at the points tested. The maximum anode efficiency is 39% ( $\pm 3\%$ ).

As described by Gascon et al. on the SPT-100 [27] the change in wall material does not significantly affect the thrust versus voltage behavior. The only differences for the ISCT200-US are observed at 200 V and below for a xenon mass flow of 1.2 mg/s. All the other points have similar results within the uncertainty of the measurement. However as seen in Fig. 3 a) the discharge current is significantly higher in the unshielded HT with graphite walls compared to the boron nitride case. This results in the behavior seen in Fig. 3 d) where the maximum efficiency is higher with ceramic than with graphite.

Like the thrust, the specific impulse dependence on voltage (Fig. 3

c)) does not appear to be strongly affected by the change in material. Interestingly the points at a mass flow of 1 mg/s are nearly indistinguishable from the one at 1.2 mg/s while the specific impulse at 0.8 mg/s is significantly lower. This suggests that a higher proportion of the propellant is not ionized at low mass flow.

An overview of the anode efficiency achieved with low power Hall thrusters is available in the appendix (Fig. 9). The ISCT200-US has performances comparable to the CAM200-EM, PlaS-40, T-40 and SPT-30. It outperforms the HT100D by about 5% under 250 W. The BHT-200 and CAMILA-HT-55 are however in a class of their own with an efficiency of more than 45% at 200 W while most other HT only get 35%.

Keeping in mind that the ISCT200-US is a laboratory thruster which has not been optimized for performances we think it adequately compares to commercial thrusters and constitute a good benchmark to assess the performances of the magnetic shielding concept.

#### 4.1.2. Magnetically shielded thruster

As show in Fig. 4 a), the change of wall material has nearly no effects on the discharge current. This is consistent with the previous results obtained in the small NEXET test chamber [24].

The measured thrust of the magnetically shielded thruster ranges from 4 to 14 mN. As seen in Fig. 4 b) the thrust of the boron nitride and graphite versions are nearly identical at 250 V and below. A slightly higher thrust is measured with graphite walls but it is within the measurement uncertainty. At 300 V the graphite outperforms the ceramic by a more significant margin.

A similar trend is seen on the specific impulse (Fig. 4 c). The measured impulse ranges between 550 and 1250 s. The graphite and ceramic versions are fairly similar until the 300 V mark where the graphite has a measured ISP around 10–15% higher than the BN-SiO<sub>2</sub>. Contrary to the US-HT the specific impulse does not reach a plateau as the mass flow is increased at constant voltage. This is indicative of a poor propellant utilization and will be discussed in more details in sections 4.2 and 4.3.

The magnetically shielded thruster only reaches 25% anode efficiency (Fig. 4 d). Once again the change of material has little effect on the performances of the MS-HT at lower discharge power. It's only above 300 W that we see a significant advantage for the graphite walls.

While this anode efficiency is rather low compared to classical unshielded Hall thrusters in the same power range (see Fig. 9), it is comparable to the MaSMi-40 and MaSMi-60-LM1 magnetically shielded Hall thrusters built by Conversano [18]. This thruster design has also not been optimized for high performance in magnetic shielding. The difference in thrust at higher voltage between the two materials is not explained for now.

#### 4.1.3. Comparison between both thrusters

Fig. 5 represents the point cloud of all the test cases done with BN-SiO<sub>2</sub> during this campaign. It is readily apparent that the unshielded thruster has a higher thrust at equivalent discharge power. The difference is more pronounced at higher discharge powers.

This result is reflected in the anode efficiency (Fig. 6). The US-HT is about 10 points higher than the MS-HT over the whole power range covered in this study.

### 4.2. Divergence and plume behavior

The divergence angles obtained in the PIVOINE 2G chamber show the same tendency as for the previous measurements in the much smaller NEXET chamber [24]. With the ceramic walls, the divergence of the unshielded thruster is slightly smaller than the MS one. We see here a 3° difference. The divergence angle of the MS-HT is nearly identical with the graphite walls while it increases dramatically in the US case.

Like the previous study [24] the propellant utilization  $\eta_{prop}$  is higher in the US-HT than in the MS-HT. However the difference is more

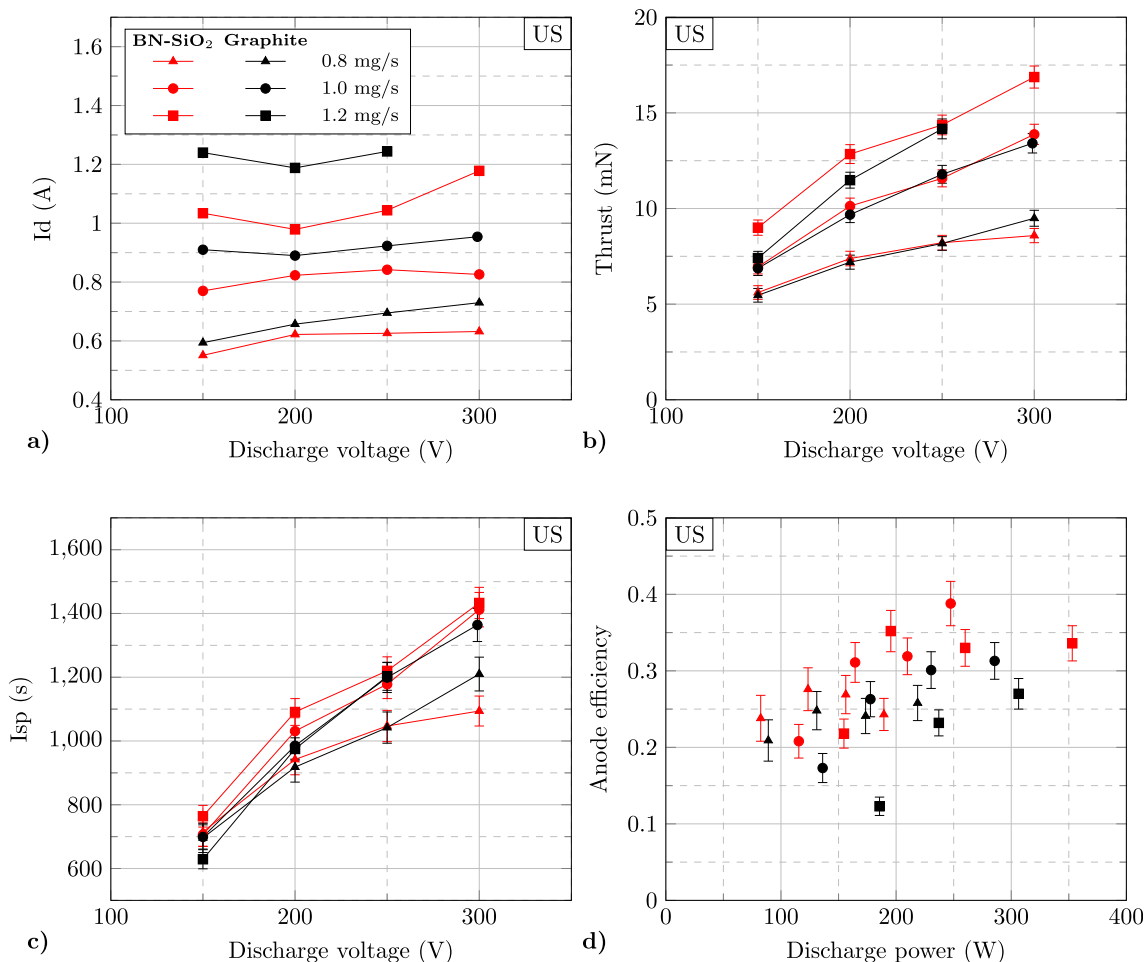


Fig. 3. Discharge current (a), thrust (b), anode specific impulse (c) and anode efficiency (d) of the ISCT200-US.

pronounced here (+10–15%) than in the other chamber (+7%). This might be due to the factor 10 in background pressure decreasing the smoothing effect of the chamber background plasma. While the thrusters were identical and the data processing was done in the same way the probe design was different. This could also explain the higher divergence angles calculated.

Compared to those earlier results a difference is seen here in the current fraction. The discharge current is the sum of the ion beam current and the electrons collected by the anode. The lower ion beam current over discharge current ratio for the MS-HT means that an important electron current is present in the shielded thruster. This result was not observed previously.

Comparing the ceramic and the graphite cases, very little variation is seen for the MS-HT. The US-HT on the other hand shows a decrease in the ion current fraction but an increase in the ionized propellant fraction for the 1.2 mg/s case.

#### 4.3. Losses in a shielded thruster

##### 4.3.1. Multiple ionization

As described in section 3.2, the results presented in section 4.2 assume that all ions are singly charged to compute the propellant utilization fraction. This approximation is not too far from the truth for traditional US-HT. The beam composition was measured to be 91% Xe<sup>+</sup>, 7% Xe<sup>2+</sup> and 2% Xe<sup>3+</sup> in the plume of the BHT-200 [36] which gives a mean ion charge of 1.11 *e*. In magnetically shielded thrusters such as the H6MS [12] and the MaSMi-60-LM1 [18] the proportion of doubly and triply charge ions is much higher. Conversano measured

61% Xe<sup>+</sup>, 25% Xe<sup>2+</sup> and 14% Xe<sup>3+</sup> in the plume of the MaSMi-60 operating at 250 W. This amounts for an average ion charge of 1.53 *e*. Replacing  $q_{mean}$  in equation (1) by those values we get a propellant efficiency of only 44% for the ISCT200-MS at 1.2 mg/s in BN-SiO<sub>2</sub> and 68% for the ISCT200-US in the same conditions (compared to 67% and 76% respectively without correcting for mean ion charge).

The high proportion of multiply charged ions in MS-HT is usually explained by the higher electron temperature in this type of thruster due to the reduced electron cooling at the walls [17].

It is tempting to explain the lower performance of the shielded thruster by this overabundance of multiply charged ions. Not only those take more energy per unit of charge to produce, but they only produce  $\sqrt{2}$  (and  $\sqrt{3}$ ) of the thrust for an equivalent acceleration voltage.

Assuming the ion population described above we can use the ionization energies for the required for the different ionization level to compute the power spent to produce them. This comes out at 13.3 W per amperes of ion current in the US-HT and 16.3 for the MS-HT. Taking for example the case of the two thrusters at 200 V and 1.2 mg/s xenon mass flow, we can calculate the power spent ionizing the ion current observed. 8.9 W is spent on ionizing the propellant for the ISCT200-US and 9.6 W is used in the ISCT200-MS. The additional energy required to produce those doubly and triply charged ions is clearly not enough to explain the difference in efficiency.

The thrust also depends on the ion charge. Neglecting the divergence and assuming the ions take advantage of 100% of the discharge voltage we can write equations (2)–(5). These equations also assume all the ions are produced at the same location.

$$T = \dot{m}_I (\eta_{Xe^+ \cdot V_{Xe^+}} + \eta_{Xe^{2+} \cdot V_{Xe^{2+}}} + \eta_{Xe^{3+} \cdot V_{Xe^{3+}}}) \quad (2)$$

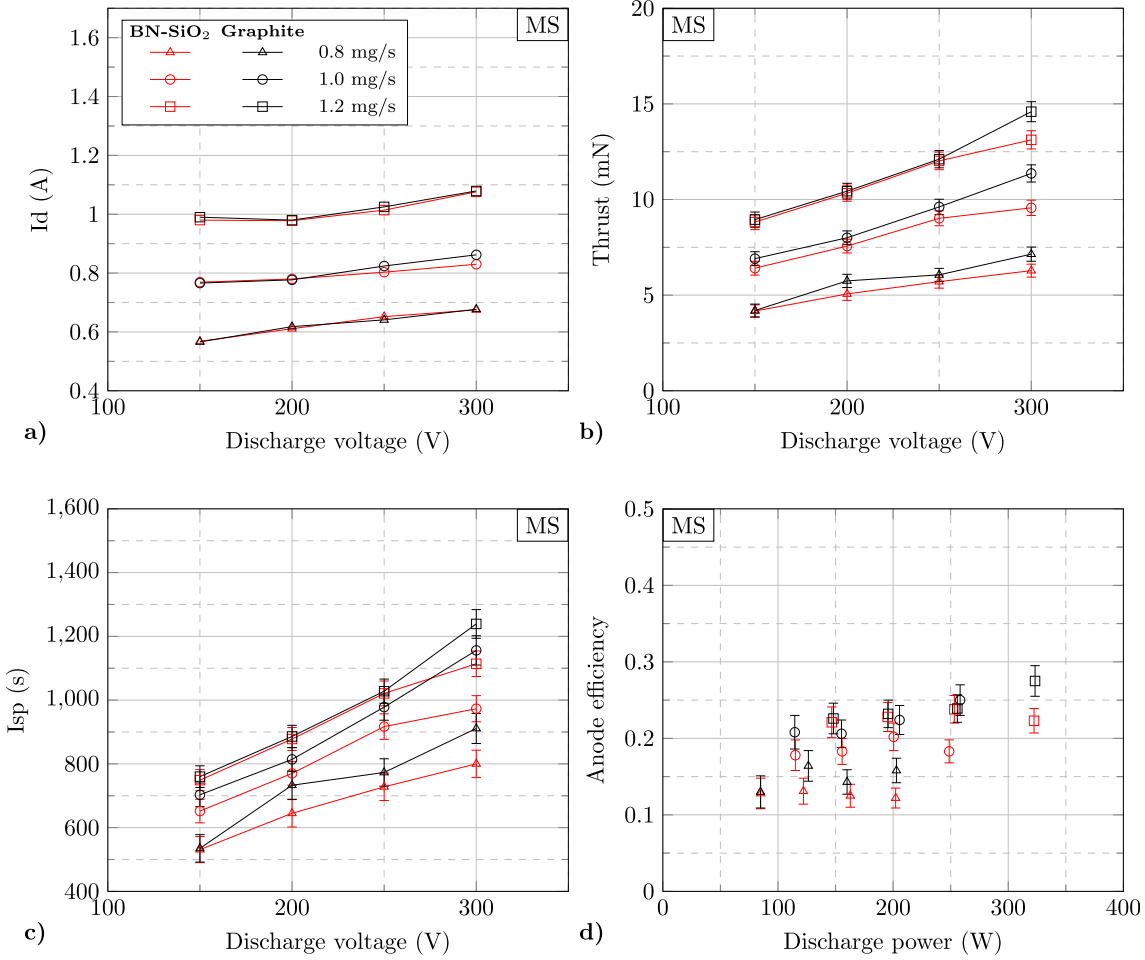


Fig. 4. Discharge current (a), thrust (b), anode specific impulse (c) and anode efficiency (d) of the ISCT200-MS.

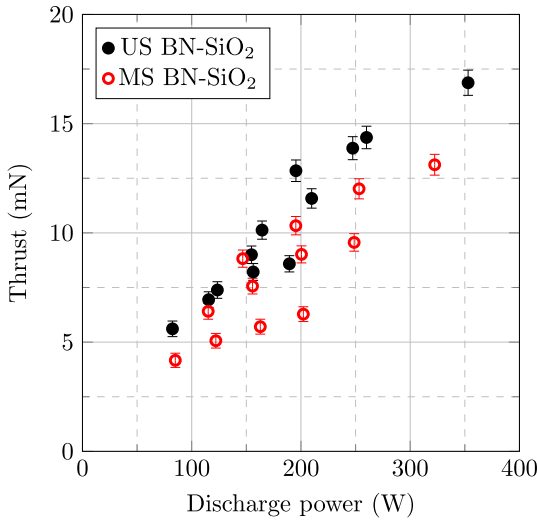


Fig. 5. Comparison between the thrust of the US and MS thrusters with ceramic wall.

$$T = \dot{m}_I \times \sqrt{\frac{2e \cdot V_d}{m_{Xe}}} \times (\eta_{Xe^+} + \sqrt{2} \cdot \eta_{Xe^{2+}} + \sqrt{3} \cdot \eta_{Xe^{3+}}) \quad (3)$$

$$T = \frac{I_b}{q_{mean}} \sqrt{2e \cdot V_d \cdot m_{Xe}} \times (\eta_{Xe^+} + \sqrt{2} \cdot \eta_{Xe^{2+}} + \sqrt{3} \cdot \eta_{Xe^{3+}}) \quad (4)$$

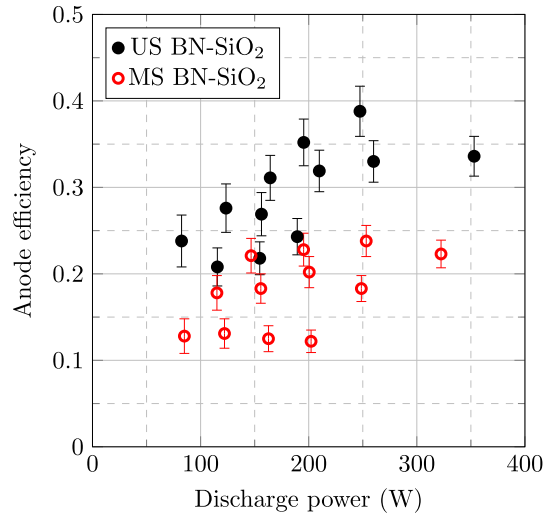


Fig. 6. Comparison between the anode efficiency of the US and MS thrusters with ceramic wall.

$$T = I_b \sqrt{\frac{2 \cdot V_d \cdot m_{Xe}}{e}} \times \frac{\eta_{Xe^+} + \sqrt{2} \cdot \eta_{Xe^{2+}} + \sqrt{3} \cdot \eta_{Xe^{3+}}}{\eta_{Xe^+} + 2 \cdot \eta_{Xe^{2+}} + 3 \cdot \eta_{Xe^{3+}}} \quad (5)$$

As a result for a given ion beam current ( $I_b$ ) a 200 W MS thruster with the ions population described above would produce only 84% of the thrust of an equivalent US thruster. All things being equal this reduces the anode efficiency by 30%. Accounting for the difference in ion

beam current for the 200 V, 1.2 mg/s, BN-SiO<sub>2</sub> case the computed thrust for the MS-HT should only be 73% of the US-HT.

At this operating point we measure a thrust of 10.3 mN for the ISCT200-MS and 12.9 mN for the ISCT200-US in the same conditions. This results in a  $80 (\pm 4.5)\%$  MS over US thrust ratio. This seems like a reasonable match with the calculation considering the uncertainty in the actual beam composition as well as the beam current.

One might then ask why the H6MS achieves an anode efficiency (0.672) so close to the unshielded H6 (0.682) [12]. First the 6 kW unshielded version of the thruster has a significantly higher fraction of multiply charged ions which adds to a mean charge of 1.27 *e* while the H6MS version is only at 1.45 *e*. This means that at equal ion beam current the thrust ratio is 92%. However the ion beam current is actually higher in the MS version (87%) than in the US version (83%). This puts the thrust ratio, only accounting for multi-charged ions and beam current fraction, at 96% which is line with the measured thrust ratio of 95.8%. Of course one should be careful with this kind of approach as it neglects divergence and potential difference in ion energy.

This simple derivation shows that while the thrust of the ISCT200-MS, like other MS thrusters, is penalized by the multiply charged ions, this effect is worsened by the low ion beam current measured in the MS-HT. The main reason for the low ion beam current in the ISCT200-MS seems to be its propellant utilization.

#### 4.3.2. Effect of surface to volume ratio

A striking characteristic of magnetically shielded Hall thrusters is the gap visible between the bulk of the plasma and the walls [37]. Fig. 7 highlights those gaps in the ISCT200-MS thruster. This less luminous area is a region of lower plasma density. This was seen with our LIF measurements near the walls [25] where we saw a sharp decrease of the ion density near the walls in the MS-HT. The US-HT on the other hand had a nearly constant ion density. Similarly surface probe measurements in the H6US and H6MS near the exit plane show a decrease of the ions current density from 12 to 5 mA/cm<sup>2</sup> [12].

We propose that this gap is a path for the neutrals to leak outside the thruster without going through the ionization area. This would explain the poor propellant utilization in the 200 MS thruster compared to the US one. It would also be consistent with the much smaller difference in propellant utilization between the H6MS and H6US. This leakage of neutral has been observed in simulations on the H6MS [17].

From the pictures of the ISCT200-MS firing we chose to assume a 1 mm gap between the plasma and the walls where no ionization take place. Under this assumption the effective ionization area would be reduced by 40% in the ISCT200 case but only by 4% in the H6.

The propellant utilization fraction shown on Table 1 are not corrected for multiply charged ions as these fractions are not known for our thruster. However as explained in section 4.3.1 we can make use of the mean ion charge measured on other comparable thrusters. Once corrected for the mean charge the propellant utilization, in our previously used reference case of 200 V, 1.2 mg/s, is 36% lower in MS than

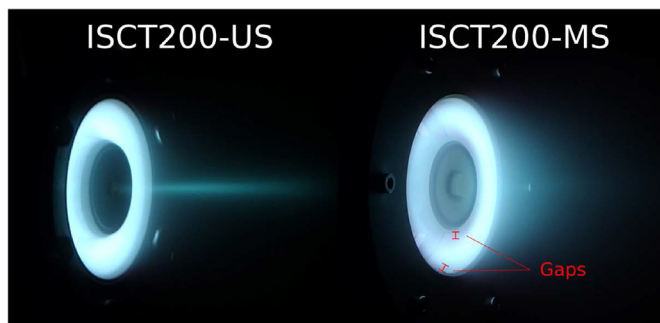


Fig. 7. Comparison of the shape of the plasma between the unshielded and shielded thrusters.

Table 1

Overview of the data derived from plume measurements. All the cases presented correspond to a 200 V discharge voltage and are not corrected for multiply charged ions.

	$\dot{m}_a$ (mg/s)	BN-SiO <sub>2</sub>			Graphite		
		$\alpha_d$ (°)	$\eta_I$	$\eta_{prop}$	$\alpha_d$ (°)	$\eta_I$	$\eta_{prop}$
MS	1.0	63	59%	60%	62	59%	63%
	1.2	62	60%	67%	61	60%	68%
US	1.0	60	68%	76%	66	63%	77%
	1.2	59	69%	76%	66	61%	82%

in US. This 36% lower propellant utilization is fairly consistent with the 40% reduction in effective ionization area. This also fits the H6MS case [12]. The shielded version of the thruster has a 2% lower propellant utilization than its unshielded counterpart while the effective ionization area is reduced by 4%.

This assumption of a 1 mm gap with no ionization is very reductionist. It supposes a uniform ionization rate across the thruster and zero ionization in the gap. This is obviously not correct as some ions where measured in the area during a previous study on the ISCT200-MS [25] and on the H6MS [12]. However the spectroscopy data seems to suggest the ion density is reduced by at least 4 at the wall in magnetic shielding. The width of the gap itself is also hard to define as it may be more or less apparent depending on the camera settings. This is especially true in the H6 where the dimensions of the thruster have to be inferred from photographic evidence.

Only two data points (ISCT200 and H6 thrusters) are available so far. However they seem consistent with a propellant loss proportional to the surface to volume ratio of the discharge channel. A smaller thruster with its large surface to volume ratio could be more sensitive to “leaks” near the channel walls than a larger one.

Conversano proposed that the poor ionization seen in the MaSMi-60-LM1 was due to non-optimal gas injection design as well as a too weak magnetic barrier [18,19]. This explanation is unsatisfying in our case as the ISCT200-MS and ISCT200-US have been tested with the same gas injection system, same magnetic field intensity and same magnetic field gradients at the center of the discharge channel. A “leak” of the neutral atoms through the gap between the plasma and the walls has the advantage of providing the right ballpark figure for the dramatic reduction in propellant utilization as well as explaining why this is not seen in larger MS thrusters such as the H6MS, NASA-300MS [38] or HERMeS [13].

#### 4.3.3. Magnetic topology

The last major difference between the MS and US thrusters is the position of the acceleration region. Previous laser induced fluorescence (LIF) spectroscopy measurements have shown that in the MS thruster the electric field is situated a few millimeters outside the discharge channel [25]. This position coincides with the position of maximum magnetic field. As illustrated in Fig. 8, in a MS-HT in order to get the magnetic field lines going from the exit plane to the anode along the walls (so called “grazing line”) this maximum needs to be pushed downstream. The gap between the exit of the discharge channel and the acceleration region could cause the slow ions to diffuse toward the magnetic poles, thus not contributing to the thrust. The losses due to this phenomenon would also be proportional to the surface over volume ratio (or more accurately in this case perimeter over surface or the exit area), further disadvantaging small MS-HT.

The external electric field can be, as a first approximation, considered to be normal to the magnetic field lines at this position. In a US-HT we take advantage of this effect by creating a “magnetic lens” that focuses the ion beam toward the center axis of the thruster and limits divergence. The shape of the magnetic field in a MS-HT imposes compromises between beam focusing and wall shielding. This is particularly

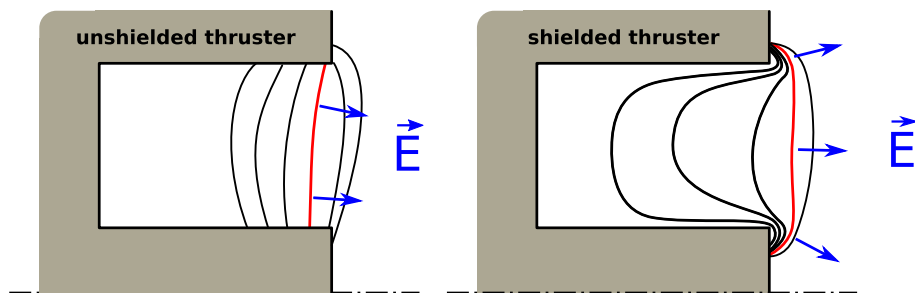


Fig. 8. Magnetic field topology and US (left) and MS (right) thrusters. The red line represents the maximum magnetic field intensity as well as the area of maximum electric field. The blue arrows show the direction of the electric field. (For interpretation of the references to colour in this figure legend, the reader is referred to the Web version of this article.)

acute in a small thruster where the magnetic field line curvature must be high in order to reach the anode area. This high curvature is also suspected to accelerate ions toward the magnetic pole causing some of the pole erosion seen on MS-HT [25,39–41].

This highly curved magnetic field with weak magnetic lensing is probably the cause of the higher divergence and hurts performances. This is presumably what Conversano calls “over-shielding” [18,19]. A compromise “low-erosion” topology, where the grazing lines do not reach as far back toward the anode would probably represent good middle ground between wall shielding and performances. Such a configuration would also certainly reduce the gap between the bulk and the plasma and the walls as well as reduce the curvature of the magnetic field lines near the poles.

## 5. Conclusion

At first glance magnetically shielded Hall thrusters seems to behave the same as classical unshielded thrusters. The change in magnetic field topology has little effect on the discharge current and, as far as kilowatt class thrusters are concerned, have similar performances.

However thrust measurement on the 200 W ISCT200 thrusters shows that the MS-HT has significantly lower thrust and anode efficiency than its US counterpart. Measurements of the plasma plume show that this difference is mainly caused by a propellant ionization in the magnetically shielded thruster. The poor ionization is somewhat compensated by the larger fraction of multiply charged ions which results in a similar discharge current.

Poor propellant utilization may be explained by the plasma not

filling the entirety of the discharge channel in a MS-HT. Those gaps in the ionization surface create a space for the neutral atoms to escape. Their effects on the thruster performance are all the more important as the thruster is small and they cover a large portion of the discharge channel. They are however negligible in larger thrusters and thus do not impact the performances as dramatically.

Previous arguments put forward by Conversano [17–19] to explain the low propellant ionization and current fraction observed in the MaSMi-60-LM1 do not seem to apply here. In those studies poor neutral injection, short channel length, weak magnetic field strength and steep magnetic field gradients were identified as the drivers behind those poor performance. However in this study these parameters were the same in both thrusters. Conversano also identified the magnetic shielding topology itself to be one possible reason for the performance measured. This is consistent with the results obtained here as only the shape of the magnetic field was changed between thrusters.

This suggests that the smaller the Hall thruster is, the bigger the performance gap between a fully magnetically shielded thruster and an equivalent standard one will be.

## Acknowledgments

This work was done as part of CNES research and development program. It has been financially supported by the CNES and the Région Centre council.

We want to thank Guillaume Largeau for his technical assistance during the test campaign on Pivoine 2G.

Appendix

5.1. Low power Hall thrusters efficiency

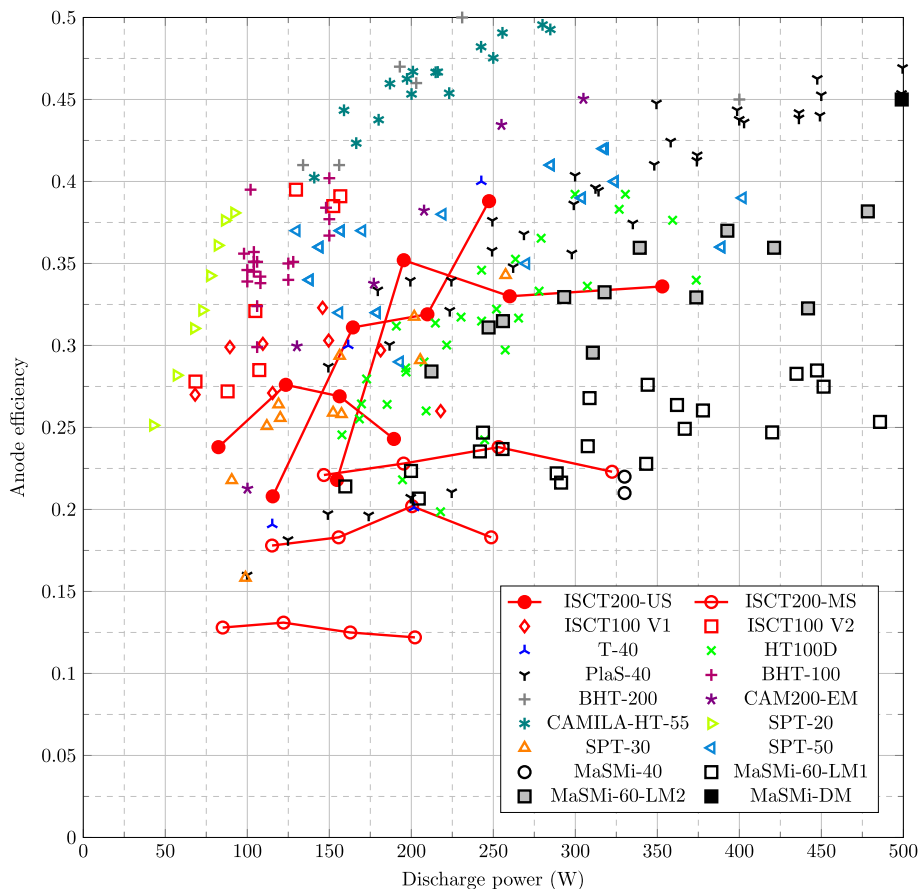


Fig. 9. Overview of the anode efficiency of low power Hall thrusters. The lines link operating points as same mass flow presented in this study.

Table 2  
Source of the data presented in Fig. 9

Thruster	Source
ISCT100 V1	Mazouffre 2018 [42]
ISCT100 V2	Unpublished
T-40	Frieman 2015 [43]
HT100D	Ducci 2013 [44]
PlaS-40	Potapenko 2015 [45]
BHT-100	Szabo 2017 [46]
BHT-200	Szabo 2012 [47]
CAM200-EM	Lev 2016 [48]
CAMILA-HT-55	Kapulkin 2011 [49]
SPT-20	Loyan 2007 [50]
SPT-30	Jacobson 1998 [51]
SPT-50	Manzella 1996 [52]
MaSMi-40	Conversano 2014 [53]
MaSMi-60-LM1	Conversano 2017 [18]
MaSMi-60-LM2	Conversano 2017 [20]
MaSMi-DM	Conversano 2017 [21]

References

[1] S. Mazouffre, Plasma Sources Sci. Technol. 25 (2016) 033002, <http://dx.doi.org/10.1088/0963-0252/25/3/033002> <http://stacks.iop.org/0963-0252/25/i=3/a=033002?key=crossref.9c6a720db6c50120415318928e7b3f98>.  
 [2] R.W. Conversano, D.M. Goebel, R.E. Wirz, Magnetically Shielded Miniature Hall Thruster, (2014) <https://patents.google.com/patent/US20150128560A1/en>.

- [3] F. Marchandise, N. Cornu, F. Darnon, E. Denis, 30th International Electric Propulsion Conference, 2007 IEPC-2007-164.
- [4] R.R. Hofer, J.E. Polk, M.J. Sekerak, I.G. Mikellides, H. Kamhawi, T.R. Sarver-Verhey, D. a. Herman, G. Williams, 52nd AIAA/SAE/ASEE Joint Propulsion Conference, American Institute of Aeronautics and Astronautics, Salt Lake City, UT, 2016, pp. 1–20, <http://dx.doi.org/10.2514/6.2016-4825> <http://arc.aiaa.org/doi/10.2514/6.2016-4825>.
- [5] I.G. Mikellides, I. Katz, R.R. Hofer, D.M. Goebel, K. de Grys, A. Mathers, *Phys. Plasmas* 18 (2011) 033501, <http://dx.doi.org/10.1063/1.3551583> <http://scitation.aip.org/content/aip/journal/pop/18/3/10.1063/1.3551583>.
- [6] A.I. Morozov, V.V. Savelyev, *Reviews of Plasma Physics* 21, Springer, US, 2000, pp. 203–391, [http://dx.doi.org/10.1007/978-1-4615-4309-1\\_2](http://dx.doi.org/10.1007/978-1-4615-4309-1_2) [http://link.springer.com/10.1007/978-1-4615-4309-1\\_2](http://link.springer.com/10.1007/978-1-4615-4309-1_2).
- [7] R.R. Hofer, R.S. Jankovsky, A.D. Gallimore, *J. Propul. Power* 22 (2006) 721–731, <http://dx.doi.org/10.2514/1.15952> <http://richard.hofer.com/pdf/hofer%7B%7D%2006%7B%7D%20part01.pdf> <http://arc.aiaa.org/doi/10.2514/1.15952>.
- [8] R.R. Hofer, A.D. Gallimore, *J. Propul. Power* 22 (2006) 732–740, <http://dx.doi.org/10.2514/1.15954> <http://arc.aiaa.org/doi/10.2514/1.15954>.
- [9] J. Geng, L. Brieda, L. Rose, M. Keidar, *J. Appl. Phys.* 114 (2013) 103305, <http://dx.doi.org/10.1063/1.4821018> <http://aip.scitation.org/doi/10.1063/1.4821018>.
- [10] J. Vaudolon, *Electric Field Determination and Magnetic Topology Optimization in Hall Thrusters*, Ph.D. thesis Université d'Orléans, 2015.
- [11] I. Mikellides, I. Katz, R. Hofer, D. Goebel, K. de Grys, A. Mathers, 46th AIAA/ASME/SAE/ASEE Joint Propulsion Conference & Exhibit, July, American Institute of Aeronautics and Astronautics, Nashville, TN, 2010, <http://dx.doi.org/10.2514/6.2010-6942> <http://arc.aiaa.org/doi/abs/10.2514/6.2010-6942>.
- [12] R. Hofer, D. Goebel, I. Mikellides, I. Katz, 48th AIAA/ASME/SAE/ASEE Joint Propulsion Conference & Exhibit, American Institute of Aeronautics and Astronautics, Reston, Virginia, 2012, <http://dx.doi.org/10.2514/6.2012-3788> <http://arc.aiaa.org/doi/abs/10.2514/6.2012-3788>.
- [13] R. R. Hofer, H. Kamhawi, D. Herman, J. E. Polk, J. S. Snyder, I. Mikellides, W. Huang, J. Myers, J. Yim, G. Williams, A. L. Ortega, B. Jorns, M. Sekerak, C. Griffiths, R. Shastry, T. Haag, T. Verhey, B. Gilliam, I. Katz, D. M. Goebel, J. R. Anderson, J. Gilland, L. Clayman, in: 34th International Electric Propulsion Conference, Kobe, Japan, pp. IEPC-2015-186.
- [14] Kathe Dannenmayer, *Scaling Laws and Electron Properties in Hall Effect Thrusters*, Ph.D. thesis Université d'Orléans, 2012.
- [15] A. Lejeune, K. Dannenmayer, G. Bourgeois, S. Mazouffre, M. Guyot, S. Denise, in: *Proceedings of the 32nd International Electric Propulsion Conference*, pp. IEPC-2011-019.
- [16] K. Dannenmayer, S. Mazouffre, *J. Propul. Power* 27 (2011) 236–245, <http://dx.doi.org/10.2514/1.48382> <http://arc.aiaa.org/doi/abs/10.2514/1.48382?journalCode=jpp> <http://arc.aiaa.org/doi/abs/10.2514/1.48382>.
- [17] R. Conversano, *Low-power Magnetically Shielded Hall Thrusters*, Ph.D. thesis University of California, Los Angeles, 2015 <http://www.escholarship.org/uc/item/4jzt1tzc>.
- [18] R.W. Conversano, D.M. Goebel, R.R. Hofer, I.G. Mikellides, R.E. Wirz, *J. Propul. Power* (2017) 1–9, <http://dx.doi.org/10.2514/1.B36230> Accepted <https://arc.aiaa.org/doi/10.2514/1.B36230>.
- [19] R.W. Conversano, D.M. Goebel, I.G. Mikellides, R.R. Hofer, R.E. Wirz, *J. Propul. Power* (2017) 1–10, <http://dx.doi.org/10.2514/1.B36231> Accepted <https://arc.aiaa.org/doi/10.2514/1.B36230> <https://arc.aiaa.org/doi/10.2514/1.B36231>.
- [20] R.W. Conversano, D.M. Goebel, R.R. Hofer, N. Arora, 2017 IEEE Aerospace Conference, IEEE, 2017, pp. 1–12, <http://dx.doi.org/10.1109/AERO.2017.7943577> <http://ieeexplore.ieee.org/document/7943577>.
- [21] R. W. Conversano, R. B. Lobbia, K. C. Tilley, D. M. Goebel, S. W. Reilly, I. G. Mikellides, R. R. Hofer, in: 35th International Electric Propulsion Conference, Atlanta, GA, pp. IEPC-2017-64.
- [22] L. Grimaud, J. Vaudolon, S. Mazouffre, C. Boniface, 52nd AIAA/SAE/ASEE Joint Propulsion Conference, American Institute of Aeronautics and Astronautics, Salt Lake City, UT, 2016, pp. 1–17, <http://dx.doi.org/10.2514/6.2016-4832> <http://arc.aiaa.org/doi/10.2514/6.2016-4832>.
- [23] L. Grimaud, J. Vaudolon, S. Mazouffre, in: *Space Propulsion Conference*, May, Rome.
- [24] L. Grimaud, S. Mazouffre, *J. Appl. Phys.* 122 (2017) 033305, <http://dx.doi.org/10.1063/1.4995285> <http://aip.scitation.org/doi/10.1063/1.4995285>.
- [25] L. Grimaud, S. Mazouffre, *Plasma Sources Sci. Technol.* 26 (2017) 055020, <http://dx.doi.org/10.1088/1361-6595/aa660d> <http://stacks.iop.org/0963-0252/26/i=5/a=055020?key=crossref.690c4a72039583e9b4b8edfe922d3a21>.
- [26] D.M. Goebel, R.R. Hofer, I.G. Mikellides, I. Katz, J.E. Polk, B.N. Dotson, *IEEE Trans. Plasma Sci.* 43 (2015) 118–126, <http://dx.doi.org/10.1109/TPS.2014.2321110> [https://moscow.sci-hub.bz/45f5e1a8392e78642a8f7edc822ce0fe/10.1109\(%\)40tps.2014.2321110.pdf](https://moscow.sci-hub.bz/45f5e1a8392e78642a8f7edc822ce0fe/10.1109(%)40tps.2014.2321110.pdf) <http://ieeexplore.ieee.org/document/6823732/>.
- [27] N. Gascon, M. Dudeck, S. Barral, *Phys. Plasmas* 10 (2003) 4123–4136, <http://dx.doi.org/10.1063/1.1611880> <http://scitation.aip.org/content/aip/journal/pop/10/10/10.1063/1.1611880> <http://aip.scitation.org/doi/10.1063/1.1611880>.
- [28] S. Barral, K. Makowski, Z. Peradzynski, N. Gascon, M. Dudeck, *Phys. Plasmas* 10 (2003) 4137, <http://dx.doi.org/10.1063/1.1611881> <http://scitation.aip.org/content/aip/journal/pop/10/10/10.1063/1.1611881>.
- [29] Y. Ding, H. Sun, W. Peng, Y. Xu, L. Wei, H. Li, P. Li, H. Su, D. Yu, *Jpn. J. Appl. Phys.* 56 (2017) 050312, <http://dx.doi.org/10.7567/JJAP.56.050312> <http://stacks.iop.org/1347-4065/56/i=5/a=050312?key=crossref.237ad9bd9b85fb62db5a3260ea2e77f3>.
- [30] Y. Ding, W. Peng, H. Sun, L. Wei, M. Zeng, F. Wang, D. Yu, *Jpn. J. Appl. Phys.* 56 (2017) 038001, <http://dx.doi.org/10.7567/JJAP.56.038001> <http://stacks.iop.org/1347-4065/56/i=3/a=038001?key=crossref.93134d38ec9a93fe872152fbbbeab3315>.
- [31] K.D. Diamant, J.E. Pollard, R.B. Cohen, Y. Raitses, N.J. Fisch, *J. Propul. Power* 22 (2006) 1396–1401, <http://dx.doi.org/10.2514/1.19417> <http://arc.aiaa.org/doi/10.2514/1.19417>.
- [32] R.D. Kolasinski, J.E. Polk, D. Goebel, L.K. Johnson, *Appl. Surf. Sci.* 254 (2008) 2506–2515, <http://dx.doi.org/10.1016/j.apsusc.2007.09.082> <http://linkinghub.elsevier.com/retrieve/pii/S0169433207014146>.
- [33] S. Mazouffre, G. Largeau, L. Garrigues, C. Boniface, K. Dannenmayer, in: *Proceedings of the 35th International Electric Propulsion Conference*, Atlanta, Georgia, pp. IEPC2017-E2336.
- [34] R. Jousot, L. Grimaud, S. Mazouffre, *Vacuum* 146 (2017) 52–62, <http://dx.doi.org/10.1016/j.vacuum.2017.09.021> <http://www.sciencedirect.com/science/article/pii/S0042207X17305535> <http://linkinghub.elsevier.com/retrieve/pii/S0042207X17305535>.
- [35] R. Jousot, G. Sary, L. Grimaud, L. Garrigues, S. Mazouffre, B. Laurent, C. Boniface, S. Oriol, F. Masson, S. A. Engines, S. Propulsion, D. Lancesur, in: 35th International Electric Propulsion Conference, Atlanta, Georgia, pp. IEPC-2017-486 Presented.
- [36] J. Ekholm, W. Hargus, 41st AIAA/ASME/SAE/ASEE Joint Propulsion Conference & Exhibit, American Institute of Aeronautics and Astronautics, Tucson, Arizona, 2005, <http://dx.doi.org/10.2514/6.2005-4405> <http://arc.aiaa.org/doi/abs/10.2514/6.2005-4405>.
- [37] S. Mazouffre, J. Vaudolon, G. Largeau, C. Henaux, A. Rossi, D. Harribey, *IEEE Transactions on Plasma Science* 42, (2014), pp. 2668–2669, <http://dx.doi.org/10.1109/TPS.2014.2331180> <http://ieeexplore.ieee.org/articleDetails.jsp?arnumber=6847144&http://ieeexplore.ieee.org/lpdocs/epic03/wrapper.htm?arnumber=6847144>.
- [38] H. Kamhawi, W. Huang, T. W. Haag, R. Shastry, G. C. Soulas, T. Smith, I. G. Mikellides, R. R. Hofer, in: 33rd International Electric Propulsion Conference, IEPC-2013-444, Washington DC, pp. 1–23.
- [39] B. Jorns, C.A. Dodson, J.R. Anderson, D.M. Goebel, R.R. Hofer, M.J. Sekerak, A. Lopez Ortega, I.G. Mikellides, 52nd AIAA/SAE/ASEE Joint Propulsion Conference, July, American Institute of Aeronautics and Astronautics, Salt Lake City, UT, 2016, pp. 1–21, <http://dx.doi.org/10.2514/6.2016-4839> <http://arc.aiaa.org/doi/10.2514/6.2016-4839>.
- [40] D.M. Goebel, B. Jorns, R.R. Hofer, I.G. Mikellides, I. Katz, 50th AIAA/ASME/SAE/ASEE Joint Propulsion Conference, American Institute of Aeronautics and Astronautics, Pasadena, CA, 2014, pp. 1–7, <http://dx.doi.org/10.2514/6.2014-3899> <http://arc.aiaa.org/doi/10.2514/6.2014-3899>.
- [41] I.G. Mikellides, A. Lopez Ortega, B. Jorns, 50th AIAA/ASME/SAE/ASEE Joint Propulsion Conference, American Institute of Aeronautics and Astronautics, Pasadena, CA, 2014, <http://dx.doi.org/10.2514/6.2014-3897> <http://arc.aiaa.org/doi/10.2514/6.2014-3897>.
- [42] S. Mazouffre, L. Grimaud, *IEEE Transactions on Plasma Science* 46, (2018), pp. 330–337, <http://dx.doi.org/10.1109/TPS.2017.2786402> <http://ieeexplore.ieee.org/document/8260564/>.
- [43] J.D. Frieman, T.M. Liu, M.L.R. Walker, J.M. Makela, A. Mathers, P.Y. Peterson, 30th International Electric Propulsion Conference, 2015, pp. 1–13, <http://dx.doi.org/10.2514/6.2016-4833>.
- [44] C. Ducci, S. Osllyak, R. Albertoni, D. Dignani, M. Andrenucci, *Alta*, 33rd International Electric Propulsion Conference, 2013, pp. 1–9.
- [45] M. Potapenko, V. Gopanchuk, S. Olotin, in: *Joint Conference of 30th International Symposium on Space Technology and Science 34th International Electric Propulsion Conference and 6th Nano-satellite Symposium*, Hyogo-kobe, Japan.
- [46] J.J. Szabo, R. Tedrake, E. Metivier, S. Paintal, Z. Taillefer, 53rd AIAA/SAE/ASEE Joint Propulsion Conference, American Institute of Aeronautics and Astronautics, Reston, Virginia, 2017, <http://dx.doi.org/10.2514/6.2017-4728> <https://arc.aiaa.org/doi/10.2514/6.2017-4728>.
- [47] J. Szabo, B. Pote, S. Paintal, M. Robin, A. Hillier, R.D. Branam, R.E. Huffmann, *J. Propul. Power* 28 (2012) 848–857, <http://dx.doi.org/10.2514/1.B34291> <http://arc.aiaa.org/doi/abs/10.2514/1.B34291?journalCode=jpp>.
- [48] D. Lev, D. Lev, R. Eytan, G. Alon, A. Warshavsky, L. Appel, R. Advanced, *D. Systems*, 66th International Astronautical Congress, 2016 IAC-15-C4.4.4.
- [49] A. Kapulkin, V. Balabanov, M. Rubanovich, E. Behar, L. Rabinovich, A. Warshavsky, Technion, Rafael, 32nd International Electric Propulsion Conference, 2011, pp. 1–14.
- [50] A. Loyal, T. Maksymenko, in: 30th International Electric Propulsion Conference, Florence, Italy, pp. IEPC-2007-100.
- [51] D.T. Jacobson, R.S. Jankovsky, AIAA/ASME/SAE/ASEE Joint Propulsion Conference and Exhibit, 34th, Cleveland, OH, July 13-15, 1998, 1998, <http://dx.doi.org/10.2514/6.1998-3792> [arxiv.org/abs/1011.1669v3](http://arxiv.org/abs/1011.1669v3) AIAA-1998-3792.
- [52] D. Manzella, S. Oleson, J. Sankovic, T. Haag, A. Semenkina, V. Kim, 32nd Joint Propulsion Conference and Exhibit, July, American Institute of Aeronautics and Astronautics, Reston, Virginia, 1996, <http://dx.doi.org/10.2514/6.1996-2736> <http://arc.aiaa.org/doi/10.2514/6.1996-2736>.
- [53] R.W. Conversano, D.M. Goebel, I.G. Mikellides, R.R. Hofer, T.S. Matlock, R.E. Wirz, I.G. Mikellides, 50th AIAA/ASME/SAE/ASEE Joint Propulsion Conference, American Institute of Aeronautics and Astronautics, Reston, Virginia, 2014, <http://dx.doi.org/10.2514/6.2014-3896> <http://arc.aiaa.org/doi/abs/10.2514/6.2014-3896> <http://arc.aiaa.org/doi/10.2514/6.2014-3896>.